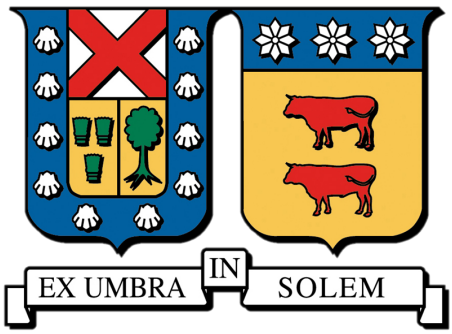


Universidad Técnica Federico Santa María

Department of Physics

# Static and Dynamic Properties of Texturized Thick Films

*Author:*
José Daniel
Jiménez Bustamante

*Thesis Director:*
Dr. Rodolfo Andrés
Gallardo Encina

A thesis submitted in partial fulfillment of the requirements for the degree of

Bachelor in science, mention physics

September, 2022

**Abstract**

The fundamental magnetic excitations, spin waves, are capable of transporting energy and angular momentum without the movement of electric charge, implying the absence of heat energy losses. Besides, the wavelengths of the spin waves are much shorter than the electromagnetic waves at the same frequency, which brings new perspectives to the miniaturization of magnonic devices. Thus, the study of the dynamic of the spin in nanostructured magnetic materials is a topic with great relevance in the area of nanomagnetism. In this thesis, a systematic study is realized to study the physics properties of a magnetic thick film that presents variations of its magnetic properties along the thickness. Due to such variations, a texturized ground state is considered, where the spin-wave modes, evaluated at zero wave vector, are calculated. Both the static and dynamic properties are calculated by using the Landau-Lifshitz equation of motion, which is solved in the linear approximation. Thus, the frequencies and the dynamic magnetization components are obtained utilizing an eigenvalue problem.

**Resumen**

Las excitaciones magnéticas fundamentales, ondas de espín, son capaces de transportar energía y momentum angular sin la necesidad de mover cargas eléctricas, implicando la ausencia de pérdida de energía por transferencia de calor. Además, la longitud de onda de las ondas de spin son mucho más cortas en comparación a las ondas electromagnéticas, brindando nuevas perspectivas para la miniaturización de dispositivos magnónicos. De este modo, el estudio the la dinámica del spin en materiales nanoestructurados magnéticos es un tópico con una gran relevancia en el nanomagnetismo. En esta tesis, se realiza un estudio sistématico para analizar las propiedades físicas the una película gruesa magnética que presenta variaciones de sus propiedades magnéticas a lo largo del grosor. Debido a estas variaciones, el estado base texturizado es considerado, donde los modos de la onda de spin, evaluadas a vector de onda cero, son calculadas. Tanto las propiedades estáticas como dinámicas son calculadas usando la ecuación de movimiento de Landau-Lifshitz, que se resuelve con una aproximación lineal. De este modo, las frecuencias y las componentes dinámicas de la magnetización son obtenidas resolviendo un problema de autovalores.

**Acknowledgements**

A mi familia por su constante amor y apoyo durante toda la vida, en especial durante la carrera y porque nunca me faltó nada para que pudiese vivir tranquilo.

A mi profesor guía Rodolfo Gallardo por su disposición, paciencia, dedicación y apoyo no-acotado durante todo este proceso.

A mis amigos, amigas y compañeros de generación por su cariño, paciencia y vida compartida durante la carrera.

Finalmente, agradecimiento al proyecto FONDECYT Regular N°1210607 que colaboró en este trabajo.

# Contents

# List of Figures

# Chapter 1

# Introduction

Nowadays, searching for new technologies and information transport is essential in society. Electronic devices are almost everywhere, but they have some problems that limit them. One is the Joule effect; the movement of charge produces heat, which means the devices lose energy[1, 2]. Besides, when trying to reduce the size of these devices to a nanometric scale, the heat will increase, and finally, the equipment will burn. For these cases, the propagation of magnetic excitations (spin waves) is an exciting window to explore and study the behavior because the non-movement of electric charges gives many possibilities to eliminate the heat problem.

The dynamic of the spin waves is often calculated over a ferromagnetic state, where the magnetic moments have the same direction. Nevertheless, under specific conditions, the magnetization can present a texture, in such a way that it can present spatial dependence. Of course, there are many possibilities to obtain a magnetic structure at small external fields. For instance, the Dzyaloshinskii-Moriya interaction (also called antisymmetric exchange) is responsible for the spontaneous formation of helicoidal and Skyrmionic structures[3, 4, 5]. Also, in some materials, stripe domains are formed to reduce the stray field[6]. Other examples are the domain walls, where the magnetization rotates between two magnetic domains [7]. Because the dynamic properties of the spin waves strongly depend on the equilibrium ground state, it is very useful to study the behavior of such waves over a magnetic ground state with a particular magnetic texture.

In this thesis, a ferromagnetic thick film is studied where a magnetic texture along the thickness is considered. The texture is induced by changing the magnetic properties along the normal of the film. The calculations associated with the texturized system are based on the Landau Lifshitz equation of motion, where the spin-wave modes, evaluated at zero wave vectors, are obtained. To consider the variation of the magnetization along the thickness, the theoretical calculations also consider applying the dynamic matrix method, where the system is subdivided into ultrathin sublayers. Thus, after a convergence test, the dynamic characteristics of the thick nanostructure are obtained.

The thesis is organized as follows: In chapter 2, the theoretical foundations of the magnetic are described, and the different interactions are listed. In chapter 3, the theory and methodology of this work are presented, showing the model, assumptions, and the effective fields for the system. The equilibrium conditions are also determined, and the system's dynamics are solved using the dynamical matrix method. In chapter 4, the main results are presented, where the ground state and frequency for different systems are studied. Finally, chapter 5 presents the conclusions of the thesis, where some discussion about future projections are commented.

# Chapter 2

# Theoretical foundations

This chapter describes the theoretical foundations of nanomagnetism. The different interactions associated with the magnetic nanostructures are illustrated, and the equation of motion of the magnetization is described.

## 2.1 Properties of the magnetic materials

Due to the motion of the electrons around the nucleus, a magnetic moment arises, which also has the contribution of the electron's spin. Therefore, the total magnetic moment is the result of the sum of the orbital and spin angular moments. This is the origin of magnetism because such magnetic moments imply that the sample will have a net magnetization. Based on the magnetic properties, the elements are classified into three main groups, namely diamagnetic, ferromagnetic, and paramagnetic.

### 2.1.1 Ferromagnetism

Ferromagnets are materials called 3d transition metals, in which the permanent elementary moments spontaneously align. Although these moments interact via their dipolar magnetic fields, the interaction giving rise to the spontaneous alignment is orders of magnitude stronger and of quantum mechanical origin. Namely, ferromagnetism can be explained through the Pauli principle due the electrons with the same spin must not be located at the same place because they would coincide in all quantum numbers. If the electrons are closer to each other, the repulsion energy or Coulomb energy will be greater. Assuming that every electron has the same spin state, so the Pauli principle forbids that the electrons are in the same place. In that case, for electrons with parallel spin, the average distance between the electrons increases, and the Coulomb energy is minimized. Therefore, using the previous assumption, it would be advantageous for metals to form parallel spins spontaneously[8]. One example is shown in figure 2.1(a).

### 2.1.2 Paramagnetism

the paramagnetism is a form of magnetism where the material is only magnetized in the presence of an externally applied magnetic field (see figure 2.1(b)). Some of the atoms or ions in the material have a net magnetic moment due to unpaired electrons in partially filled orbitals. However, the individual magnetic moments do not interact magnetically and when the field is removed, the magnetization is zero[9].

### 2.1.3 Diamagnetism

Materials that do not contain atoms or ions with permanent magnetic moments respond to an applied field with an induced magnetization that is opposed to the applied field and are called diamagnets, as depicted in figure 2.1(c). The response of a diamagnetic material to an externally applied magnetic field can be described in terms of a microscopic application of Lenz's law. As a magnetic field is applied to such a material, electronic orbital motions are modified so as to generate an opposing magnetic field[9]. Diamagnetic contributions in electrical insulators come from bound electrons circulating in atomic orbitals. Classically, the diamagnetic contribution from

conduction electrons in metals and semiconductors can be shown to vanish in thermal equilibrium. There is, however, a small non-vanishing diamagnetic effect from conduction electrons that arises from the quantization of angular momentum. Isotropic diamagnets are characterized by a negative scalar susceptibility since the induced moments oppose the applied field. Virtually all materials have a diamagnetic contribution to their total response to a magnetic field. In materials containing permanent magnetic moments, however, the diamagnetic contribution is usually overshadowed by the response of those moments[9].

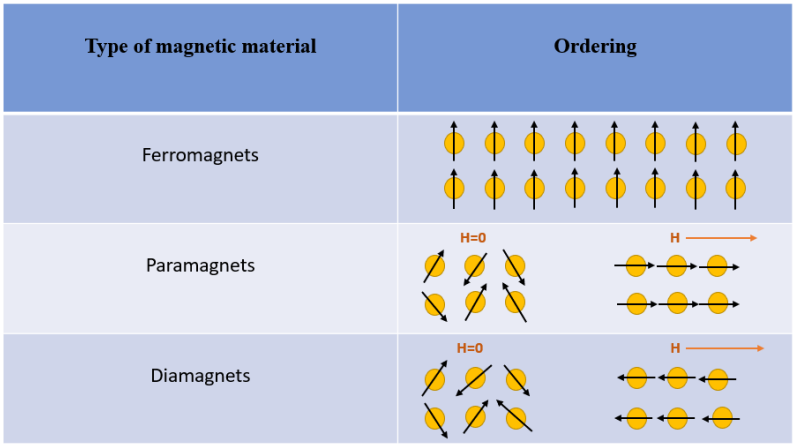


Figure 2.1: Ordering of the magnetic moments in three typical magnetic materials; namely ferromagnets, paramagnets, and diamagnets.

It is worth mentioning that there are other kind of materials that present particular magnetic configurations, for instance: Ferrimagnets, Antiferromagnets, helicoidal structures, etc. Nevertheless, they are not relevant in this thesis and, hence, are not discussed in detaild.

## 2.2 Magnetic Energies

### 2.2.1 Zeeman energy

Suppose the magnetized sample is in the presence of an external magnetic field $\mathbf{H}_0$. In that case, the magnetic moments of the sample will interact with the external field, and the parallel alignment of the magnetization $\mathbf{M}$ and the field $\mathbf{H}_0$ is the low energy state. This interaction is called Zeeman energy, and the corresponding energy density is given by[9]:

$$\epsilon_0 = -\mu_0 \mathbf{M} \cdot \mathbf{H}_0. \tag{2.1}$$

### 2.2.2 Magnetocristalline Anisotropy

Magnetocristalline anisotropy means that a ferromagnetic sample prefers energetically specific directions of magnetization[1]. The preferred directions are determined by the symmetries and structures of the crystal lattice[10]. One of the origins of the anisotropy in magnetically ordered crystals is the magnetic interaction of elementary magnetic moments. The most common anisotropy effect is connected to the existence of one only easy direction, and in literature it is referred to as uniaxial anisotropy. Thus, the anisotropy free energy density $\epsilon_{\text{an}}$ $(\mathbf{M})$ will be rotationally-symmetric with respect to the easy axis and will depend only on the relative orientation of $\mathbf{M}$ with respect to this axis. It supposed, for sake of simplicity, that the easy direction coincides with the cartesian axis $z$. Therefore, the expression of $\epsilon_{\text{u}}(\mathbf{M})$ can be written as an even function of $m_z = \cos\theta$, or equivalently using as independent variable $m_x^2 + m_y^2 = 1 - m_z^2 = \sin\theta$. This expression, developed in power series assumes the following form[1]:

$$\epsilon_{\text{u}}(\mathbf{M}) = K_0 + K_1 \sin^2\theta + K_2 \sin^4\theta + K_3 \sin^6\theta + \ldots, \tag{2.2}$$

where $K_1$, $K_2$, $K_3, \ldots$, are the anisotropy constants having the dimensions of energy per unit volume [J/m$^3$].

### 2.2.3 Demagnetizing field

An essential contribution of energy in this system is the demagnetization energy. This energy's origin is due to Maxwell's equations in a spontaneously magnetized body. As seen in electrodynamics courses, the magnetic field in vacuum or magnetic induction $\mathbf{B}$ can be described by two quantities, the magnetic field in matter $\mathbf{H}$ and the magnetization $\mathbf{M}$. The relationship among these expressions is [11]:

$$\mathbf{B} = \mu_0(\mathbf{H} + \mathbf{M}). \tag{2.3}$$

Furthermore, the second law of Maxwell expressed $\mathbf{B}$ as:

$$\nabla \cdot \mathbf{B} = 0. \tag{2.4}$$

The magnetic field $\mathbf{H}$ is, unlike the magnetic field $\mathbf{B}$, non-source free. Substituting equation 2.3 into equation 2.4 it is obtained a relationship between $\mathbf{H}$ and $\mathbf{M}$, namely

$$\nabla \cdot \mathbf{H} = -\nabla \cdot \mathbf{M}. \tag{2.5}$$

The $\mathbf{H}$-field can be discomposed into two fields[10].

$$\mathbf{H} = \mathbf{H}_0 + \mathbf{H}_{\text{dem}}, \tag{2.6}$$

where $\mathbf{H}_0$ is the external field caused by currents or external fields/ magnets meanwhile the second field $\mathbf{H}_{\text{dem}}$ is the demagnetizing field inside the sample. This decomposition is done for a particular reason, and it is possible to set the demagnetizing field as a conservative field, which means it is possible to define this field as a gradient of potential generated by magnetic charges. Using the first law of Maxwell's equations, but now the magnetic charges are given by[11]

$$\rho = -\nabla \cdot \mathbf{M}. \tag{2.7}$$

In homogeneously magnetized samples, the magnetic charges are located on the interface due the gradient of the magnetization is not zero. Using Lenz's law, the demagnetizing field must act opposite to the magnetization. For ellipsoidal homogeneously magnetized samples, the demagnetizing field can be calculated precisely. It turns out that the demagnetizing field is linearly related to the magnetization and, therefore, also homogeneous[1, 10].

$$\mathbf{H}_{\text{dem}} = -\mathcal{N}\mathbf{M}, \tag{2.8}$$

where $\mathcal{N}$ is the demagnetization tensor with trace $Tr(\mathcal{N}) = 1$[1]. For a thin, widely extended film, the length, and width are much larger than the thickness. Therefore, the components of the demagnetizing field parallel to the surface ($x$ and $y$ directions) can be neglected since the magnetic charges are very far apart [1]. This corresponds to $\mathcal{N}_{xx} = 0$ and $\mathcal{N}_{yy} = 0$. Since the trace of the demagnetization tensor is one, $\mathcal{N}_{zz} = 1$ must apply. Then, its easy to show that

$$\epsilon_{\text{dem}} = \frac{1}{2}\mu_0 \mathbf{M} \cdot \mathbf{H}_{\text{dem}}. \tag{2.9}$$

### 2.2.4 Exchange energy

It is known from quantum mechanics that the form of a wave function and, consequently, the mean energy of the Coulomb interaction of two electrons depend on the mutual orientation of their spins. The part of the Coulomb energy that depends on this orientation is called exchange energy. This energy is the cause of the magnetic ordering, mentioned in 2.1. The simplest way to express the exchange energy is through Heisenberg Hamiltonian[9, 8]:

$$\mathcal{H} = -2\frac{\mathcal{J}}{\hbar^2}\mathbf{S}_1 \cdot \mathbf{S}_2 \tag{2.10}$$

Here, $\mathbf{S}_1$ and $\mathbf{S}_2$ are angular momentum operators and $\mathcal{J}$ is the exchange constant. This interaction is described in discrete form, nevertheless in the continuous case it is easy to show that such exchange energy becomes

$$\epsilon_{\text{exc}} = \frac{A_{\text{ex}}}{M_{\text{s}}^2}\left[(\nabla M_x)^2 + (\nabla M_y)^2 + (\nabla M_z)^2\right] \tag{2.11}$$

where $A_{\text{ex}}$ is the exchange constant, and $M_{\text{s}}$ is the saturation magnetization.

## 2.3 Effective fields

For further theoretical considerations, the effective magnetic field $\mathbf{H}^{\mathrm{e}}$ is of great importance. It is calculated by forming the gradient of the total energy density with respect to the coordinates of the magnetization $\mathbf{M}$[1], namely

$$\mu_0 \mathbf{H}^{\mathrm{e}} = -\frac{1}{M_s} \nabla_{\mathbf{M}} \epsilon \tag{2.12}$$

where $\epsilon$ is the sum of the energy densities previously mentioned.

## 2.4 Landau-Lifshitz equation

In this section, some aspects of the magnetization motion are commented on. Under the presence of an effective field, the magnetization will be deflected from its equilibrium position. As a result, the magnetization will precess around such a field. During this process, the magnetization will return to the equilibrium position through a spiral movement, as shown in figure 2.2. Note that after a time, the magnetization reaches the direction of the effective field. This effect is due to intrinsic damping of the system. The time scale for this phenomenon is in the nanosecond range [1]. This behavior was studied and described theoretically by Landau and Lifshitz in 1935 [1]. The Landau-Lifshitz (LL) equation describes the precession (without damping) of the magnetization around the effective field[9]. This equation is

$$\frac{d\mathbf{M}}{dt} = -\gamma \mu_0 \mathbf{M} \times \mathbf{H}^{\mathrm{e}}, \tag{2.13}$$

here, $\gamma$ is the gyromagnetic ratio, representing the relation between the magnetic moment and angular momentum.

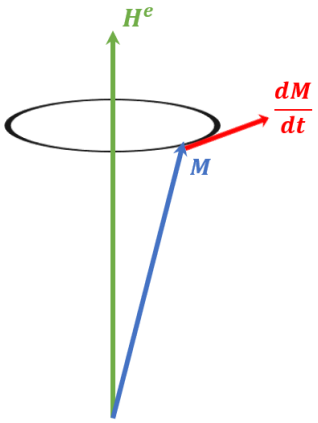


Figure 2.2: Representation of the trajectory of the magnetization motion.

An essential feature of the LL equation is that it ensures the conservation of the vector $\mathbf{M}$ length. Indeed, multiplying both sides of equation 2.13 by $\mathbf{M}$ it is found:

$$\frac{\partial}{\partial t} \mathbf{M}^2 = 0. \tag{2.14}$$

It is worth mentioning that from the LL equation of motion, the equilibrium states are also obtained. These states are calculated from the condition $\mathbf{M} \times \mathbf{H}^{\mathrm{e}} = 0$.

### 2.4.1 Ferromagnetic resonance

In typical ferromagnetic resonance experiments, the magnetization is excited by a high-frequency magnetic field in the microwave range. At the same time, the sample is exposed to the presence of an external time-independent magnetic field $\mathbf{H}_0$. At a given field $\mathbf{H}_0 = \mathbf{H}_{\mathrm{FMR}}$ and microwave frequency $\omega$, the sample absorbs the energy of the microwave irradiation. This phenomenon is called

ferromagnetic resonance (FMR), and it is very useful to characterize the sample and understand the fundamental physics behind the system.

From a calculations point of view, the frequency that matches with the one obtained from ferromagnetic resonance experiments is simply the frequency of the spin waves evaluated at zero wave vector. Such spin waves are calculated for slight deviations around the equilibrium, which is consistent with the ferromagnetic resonance setup since such an experimental technique is a perturbative method in the sense that it measures magnetic excitations with small magnetization oscillation amplitudes. Additional details are given in the next chapter, where the dynamics of a multilayer system are solved using the LL equation of motion.

# Chapter 3

# Theory for texturized thick films

The present chapter reviews the theory related to the thesis work. The LL equation is solved with the pertinent reference system, where the static and dynamic properties are analyzed. Finally, the dynamical matrix method is explained, which allows for obtaining the frequencies of the system.

### 3.0.1 Reference system

The diagram of the multilayer structure is shown in Fig 3.1. The system is composed of different ferromagnetic layers that have in-plane homogeneous magnetization. The thickness of each layer is $b$, while the equilibrium magnetization of the $\eta$-th layer makes an angle $\psi_\eta$ with respect to the $x$ axis (see figure 3.1). The local coordinates system $(X_\eta, Y_\eta, Z_\eta)$ is defined for each layer $(\eta = 1, 2, \ldots, N)$, where the magnetization of the $\eta$-th layer, $\mathbf{M}^{(\eta)}$, is pointing along $X_\eta$. The field $\mathbf{H}_0$ corresponds to the external field.

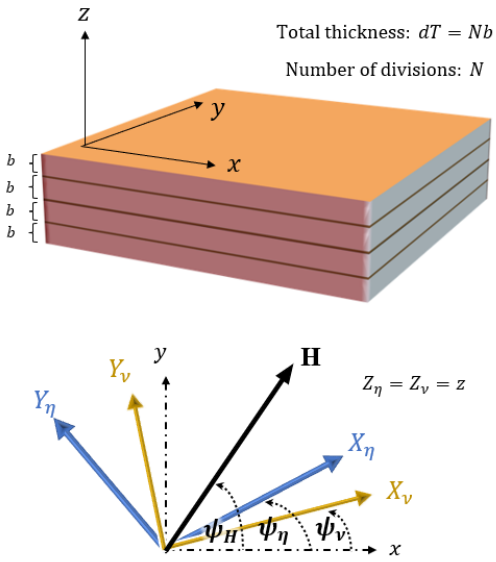


Figure 3.1: (a) Overview of the system. Coordinates $(x, y, z)$ are fixed, where $z$ is normal to the film's plane, and the thicknesses of each layer is $b$. (b) Local coordinates $(X_\eta, Y_\eta, Z_\eta)$ are defined according to the equilibrium magnetization of layer $(\eta)$.

The temporal evolution of the system is given by

$$\dot{\mathbf{M}}^{(\eta)}(\mathbf{r}, t) = -\gamma \mathbf{M}^{(\eta)}(\mathbf{r}, t) \times \mathbf{H}^{e(\eta)}(\mathbf{r}, t), \tag{3.1}$$

where the dot denotes time derivative, $\gamma$ is the absolute value of the gyromagnetic ratio, and $\mathbf{H}^{e(\nu)}(\mathbf{r}, t)$ is the effective field acting on layer $\eta$. For this thesis, the linearization approach is used,

where small deviations of the magnetization around the equilibrium are considered, and hence

$$\begin{aligned} \mathbf{M}^{(\eta)}(\mathbf{r},t) = &\quad M_{\mathrm{s}}^{(\eta)}\hat{X}_\eta + \mathbf{m}(\mathbf{r},t), \\ \mathbf{H}^{\mathrm{e}(\eta)}(\mathbf{r},t) = &\quad H_{X_\eta}^{\mathrm{e}0}\hat{X}_\eta + \mathbf{h}^{\mathrm{e}}(\mathbf{r},t), \end{aligned} \tag{3.2}$$

where $M_{\mathrm{s}}^{(\eta)}$ is the saturation magnetization of layer $\eta$, $H_{X_\eta}^{e0}$ is the $X_\eta$ component of the zero-order effective field. $\mathbf{m}(\mathbf{r},t)$ and $\mathbf{h}^{\mathrm{e}}(\mathbf{r},t)$ are the dynamic magnetizations and effective fields, respectively. Then, the dynamic magnetization is written as

$$\mathbf{m}(\mathbf{r},t) = \mathbf{m}(\mathbf{r})e^{i\omega t},$$

where $\omega = 2\pi f$, being $f$ the frequency. Finally, the LL equation of motion becomes

$$\begin{aligned} i\frac{\omega}{\gamma}m_{Y_\eta} &= -m_{Z_\eta}H_{X_\eta}^{\mathrm{e}0} + M_{\mathrm{s}}^{(\eta)}h_{Z_\eta}^{\mathrm{e}}, \\ i\frac{\omega}{\gamma}m_{Z_\eta} &= m_{Y_\eta}H_{X_\eta}^{\mathrm{e}0} - M_{\mathrm{s}}^{(\eta)}h_{Y_\eta}^{\mathrm{e}}. \end{aligned} \tag{3.3}$$

Here, it has been assumed that $H_{Z_\eta}^{\mathrm{e}0} = 0$ because the in-plane case is considered so that there are no static fields along the normal direction. Also, $H_{Y_\eta}^{\mathrm{e}0} = 0$ due the equilibrium conditions.[12]. On the other side, the effective field is the sum of the different energetic contributions of the system. Thus, it can be stated as $\mathbf{H}^{\mathrm{e}} = \mathbf{H}_0 + \mathbf{H}_{\mathrm{dem}} + \mathbf{H}_{\mathrm{u}} + \mathbf{H}_{\mathrm{ex}}$. The expressions of these fields are derived in the following section.

### 3.0.2 Effective fields

Considering the equation (2.12), it is necessary to derive the density energy $\epsilon$ to find both the contributions of static and dynamic components of the effective field.

#### Zeeman field

Using the energy density expressed in equation (2.1) and taking into account the geometry of the system, the components of the Zeeman field are

$$H_{X_\eta}^0 = H\cos(\psi_H - \psi_\eta) \tag{3.4}$$

and

$$H_{Y_\eta}^0 = H\sin(\psi_H - \psi_\eta). \tag{3.5}$$

The last contribution ($H_{Y_\eta}^0$) is crucial because it will be part of the equilibrium condition that allows calculating the equilibrium angles.

#### Anisotropy field

For the system shown in figure 3.1, it is assumed an uniaxial anisotropy with an easy axis along $y$. So, the energy density will be

$$\epsilon_{\mathrm{u}}^{(\eta)} = -\frac{H_{\mathrm{u}}^{(\eta)}}{2M_{\mathrm{s}}^{(\eta)}}\left[\mathbf{M}^{(\eta)}(x)\cdot\hat{y}\right]^2, \tag{3.6}$$

where $H_{\mathrm{u}}^{(\eta)} = 2K_{\mathrm{u}}^{(\eta)}/M_{\mathrm{s}}^{(\eta)}$.Using the expression of $\hat{y}$ in local coordinates, it is obtained that

$$\hat{y} = cos\psi\hat{Y} + \sin\psi\hat{X}$$

So, doing the dot product, the following expression of energy density is derived

$$\epsilon_{\mathrm{u}}^{(\eta)} = -\frac{\mu_0 H_{\mathrm{u}}^{(\eta)}}{2M_{\mathrm{s}}^{(\eta)}}\left[m_{Y_\eta}(x)\cos\psi_\eta + M_{X_\eta}\sin\psi_\eta\right]^2.$$

Using the equation 2.12, the static and dynamic components of the effective field are

$$H_{X_\eta}^{\mathrm{u}0} = H_{\mathrm{u}}^{(\eta)}\sin^2\psi_\eta, \tag{3.7}$$

$$H_{Y_\eta}^{\mathrm{u}0} = H_{\mathrm{u}}^{(\eta)} \sin\psi_\eta \cos\psi_\eta \tag{3.8}$$

and

$$h_{Y_\eta}^{\mathrm{u}}(x) = \frac{H_{\mathrm{u}}^{(\eta)}}{M_{\mathrm{s}}^{(\eta)}} m_{Y_\eta}(x) \cos^2\psi_\eta \tag{3.9}$$

**Demagnetizing field**

As expressed in (2.8), the demagnetizing field can be written as

$$\mathbf{H}_{\mathrm{dem}} = -\mathcal{N}\mathbf{M}. \tag{3.10}$$

Due to the geometrical configuration of the system, the tensor $\mathcal{N}$ becomes diagonal, and only the term $\mathcal{N}_{zz}$ is not null, and, hence, the field becomes simply as[1]

$$\mathbf{H}_{\mathrm{dem}} = -4\pi\mathbf{M}_{Z_\eta}$$

Thus, the field is expressed as

$$\mathbf{h}_{\mathrm{dem}} = -4\pi m_{Z_\eta}\hat{Z}. \tag{3.11}$$

**Exchange field**

The interlayer exchange, energy per unit area, between two neighboring layers is[12]

$$\epsilon_{\mathrm{ex}}^{(\eta\nu)} = -J\frac{\mathbf{M}^{(\eta)}\cdot\mathbf{M}^{(\nu)}}{M_{\mathrm{s}}^{(\eta)}M_{\mathrm{s}}^{(\nu)}} \tag{3.12}$$

Then, to obtain the components for the static and dynamics exchange fields, it is necessary to project the basis of layer $\nu$ into layer $\eta$. Using Fig 3.1 as a reference and with some trigonometry, it is obtained that

$$\begin{aligned} \hat{X}_\nu = &\quad \cos(\psi_\nu - \psi_\eta)\hat{X}_\eta - \sin(\psi_\nu - \psi_\eta)\hat{Y}_\eta, \\ \hat{Y}_\nu = &\quad \sin(\psi_\nu - \psi_\eta)\hat{X}_\eta + \cos(\psi_\nu - \psi_\eta)\hat{Y}_\eta. \end{aligned} \tag{3.13}$$

Therefore, the magnetization $\mathbf{M}^{(\nu)}$ can be written in terms of the coordinates $(X_\eta, Y_\eta, Z_\eta)$. Thus, the energy density becomes

$$\begin{aligned} \epsilon_{\mathrm{ex}}^{(\eta\nu)} = -\frac{J}{M_{\mathrm{s}}^{(\eta)}M_{\mathrm{s}}^{(\eta)}}&(M_{\mathrm{s}}^{(\eta)}M_{\mathrm{s}}^{(\nu)}\cos(\psi_\nu - \psi_\eta) + M_{\mathrm{s}}^{(\eta)}m_{Y_\nu}\sin(\psi_\nu - \psi_\eta) \\ &- m_{Y_\eta}M_{\mathrm{s}}^{(\nu)}\sin(\psi_\nu - \psi_\eta) + m_{Y_\eta}m_{Y_\nu}\cos(\psi_\nu - \psi_\eta) + m_{Z_\eta}m_{Z_\nu}) \end{aligned}$$

Similar to the previous cases, this energy density allows for obtaining effective fields. In this case, the effective exchange field components are

$$\begin{aligned} h_{Z_\eta}^{\mathrm{ex}(\eta)}(\mathbf{r},t) &= \sum_\nu \left(\delta_{\eta+1}^\nu + \delta_{\eta-1}^\nu\right)\frac{J}{b\mu_0 M_{\mathrm{s}}^{(\eta)}M_{\mathrm{s}}^{(\nu)}} m_{Z_\nu}^{(\nu)}(\mathbf{r},t) \\ h_{Y_\eta}^{\mathrm{ex}(\eta)}(\mathbf{r},t) &= \sum_\nu \left(\delta_{\eta+1}^\nu + \delta_{\eta-1}^\nu\right)\frac{J}{b\mu_0 M_{\mathrm{s}}^{(\eta)}M_{\mathrm{s}}^{(\nu)}} \cos(\psi_\eta - \psi_\nu) m_{Y_\nu}^{(\nu)}(\mathbf{r},t) \end{aligned}$$

and

$$H_X^{\mathrm{ex}0(\eta)}(\mathbf{r}) = \sum_\nu \left(\delta_{\eta+1}^\nu + \delta_{\eta-1}^\nu\right)\frac{J}{b\mu_0 M_{\mathrm{s}}^{(\eta)}} \cos(\psi_\eta - \psi_\nu) \tag{3.14}$$

$$H_Y^{\mathrm{ex}0(\eta)}(\mathbf{r}) = \sum_\nu \left(\delta_{\eta+1}^\nu + \delta_{\eta-1}^\nu\right)\frac{J}{b\mu_0 M_{\mathrm{s}}^{(\nu)}} \sin(\psi_\eta - \psi_\nu) \tag{3.15}$$

### 3.0.3 Equilibrium position

To find the equilibrium position is necessary to solve the system of equations formed by the statics fields in the $Y$-direction under the condition $H^{e0}_{Y_\eta} = 0$. Thus, the equilibrium equations will be given by

$$\begin{aligned}
H\sin(\psi_H - \psi_1) + \frac{H_u^{(1)}}{2}\sin(2\psi_1) - \frac{J}{bM_s^{(1)}}\sin(\psi_1 - \psi_2) &= 0 \\
H\sin(\psi_H - \psi_2) + \frac{H_u^{(2)}}{2}\sin(2\psi_2) - \frac{J}{bM_s^{(2)}}\sin(\psi_2 - \psi_3) - \frac{J}{bM_s^{(2)}}\sin(\psi_2 - \psi_1) &= 0 \\
&\vdots \\
H\sin(\psi_H - \psi_N) + \frac{H_u^{(N)}}{2}\sin(2\psi_N) - \frac{J}{bM_s^{(N)}}\sin(\psi_N - \psi_{N-1}) &= 0.
\end{aligned} \tag{3.16}$$

Here, $N$ represents the number of layers (or sublayers) of the sample. To solve this system of equations, it is necessary to do it numerically with proper software. Also, note that these equations are transcendentals, so it is not feasible to obtain the angles analytically.

## 3.1 Dynamical matrix method

Once the equilibrium angles are obtained, the equations (3.3) can now be solved. For this purpose, it is possible to express (3.3) as an eigenvalue problem

$$i\frac{\omega}{\gamma}\mathbf{m} = \mathcal{W}\mathbf{m}, \tag{3.17}$$

where $\omega = 2\pi f$. Here, the transpose of eigenvector $\mathbf{m}$ is

$$\mathbf{m}^T = [m_{Y_1}, m_{Z_1}, m_{Y_2}, m_{Z_2}, ..., m_{Y_N}, m_{Z_N}]$$

On the other hand, $\mathcal{W}$ has block form, namely

$$\begin{pmatrix}
W_{Y_1Y_1} & W_{Y_1Z_1} & W_{Y_1Y_2} & W_{Y_1Z_2} & \cdots\cdots \\
W_{Z_1Y_1} & W_{Z_1Z_1} & W_{Z_1Y_2} & W_{Z_1Z_2} & \cdots\cdots \\
W_{Y_2Y_1} & W_{Y_2Z_1} & W_{Y_2Y_2} & W_{Y_2Z_2} & \cdots\cdots \\
W_{Z_2Y_1} & W_{Z_2Z_1} & W_{Z_2Y_2} & W_{Z_2Z_2} & \cdots\cdots \\
\vdots & \vdots & \vdots & \vdots & \\
\vdots & \vdots & \vdots & \vdots &
\end{pmatrix}.$$

The elements of the matrix $\mathcal{W}$ have been highlighted into a matrix of 2x2 size. The matrices highlighted in blue represent intralayer interactions associated with each layer. Meanwhile, the matrices highlighted in green represent the interlayer interactions between the FM layers. These interlayer elements have an exchange nature and are fundamental in describing the system's dynamics.

The $X_\eta$ component of the effective field is

$$H^{e0}_{X_\eta} = H\cos(\psi_H - \psi_\eta) + H_u^{(\eta)}\sin^2\psi_\eta + \sum_\nu \left(\delta^\nu_{\eta+1} + \delta^\nu_{\eta-1}\right)\frac{J}{b\mu_0 M_S^{(\eta)}}\cos(\psi_\eta - \psi_\nu). \tag{3.18}$$

On the other side, the dynamic effective fields can be written as

$$h^e_{\xi_\eta}(\mathbf{r}) = \sum_{\xi'}\sum_\nu \Gamma_{\xi_\eta,\xi'_\nu} m_{\xi'_\nu}, \tag{3.19}$$

where $\xi = Y, Z$. To fill up the dynamic matrix $\mathcal{W}$, there are two cases to analyze. The first one is $\eta = \nu$, which corresponds to intralayer interactions. The second one is $\eta \neq \nu$, where interlayer exchange interactions are considered. Thus, the matrix elements can be expressed as

$$W_{Y_\eta Y_\eta} = M_s^{(\eta)}\Gamma_{Z_\eta,Y_\eta}, \tag{3.20}$$

$$W_{Z_\eta Z_\eta} = -M_{\mathrm{s}}^{(\eta)} \Gamma_{Y_\eta, Z_\eta}, \tag{3.21}$$

$$W_{Y_\eta Z_\eta} = M_{\mathrm{s}}^{(\eta)} \Gamma_{Z_\eta, Z_\eta} - H_{X_\eta}^{\mathrm{e0}}, \tag{3.22}$$

$$W_{Z_\eta Y_\eta} = -M_{\mathrm{s}}^{(\eta)} \Gamma_{Y_\eta, Y_\eta} + H_{X_\eta}^{\mathrm{e0}}. \tag{3.23}$$

and

$$W_{Y_\eta Y_\nu} = M_{\mathrm{s}}^{(\eta)} \Gamma_{Z_\eta, Y_\nu}, \tag{3.24}$$

$$W_{Z_\eta Z_\nu} = -M_{\mathrm{s}}^{(\eta)} \Gamma_{Y_\eta, Z_\nu}, \tag{3.25}$$

$$W_{Y_\eta Z_\nu} = M_{\mathrm{s}}^{(\eta)} \Gamma_{Z_\eta, Z_\nu}, \tag{3.26}$$

$$W_{Z_\eta Y_\nu} = -M_{\mathrm{s}}^{(\eta)} \Gamma_{Y_\eta, Y_\nu}. \tag{3.27}$$

Here, finally, the $\Gamma_{\xi_\eta, \xi'_\nu}$ terms are given by

$$\Gamma_{Z_\eta, Y_\eta} = 0 \tag{3.28}$$

$$\Gamma_{Y_\eta, Z_\eta} = 0 \tag{3.29}$$

$$\Gamma_{Z_\eta, Z_\eta} = -4\pi \tag{3.30}$$

$$\Gamma_{Y_\eta, Y_\eta} = \frac{H_{\mathrm{u}}^{(\eta)}}{M_{\mathrm{s}}^{(\eta)}} \cos(\psi_\eta)^2 \tag{3.31}$$

$$\Gamma_{Z_\eta, Y_\nu} = 0 \tag{3.32}$$

$$\Gamma_{Y_\eta, Z_\nu} = 0 \tag{3.33}$$

$$\Gamma_{Z_\eta, Z_\nu} = \frac{J}{b\mu_0 M_{\mathrm{s}}^{(\eta)} M_{\mathrm{s}}^{(\nu)}} \cos(\psi_\eta - \psi_\nu) \tag{3.34}$$

$$\Gamma_{Y_\eta, Y_\nu} = \frac{J}{b\mu_0 M_{\mathrm{s}}^{(\eta)} M_{\mathrm{s}}^{(\nu)}} \tag{3.35}$$

# Chapter 4

# Results

This chapter comprises the main results of the thesis. The static and dynamic properties are calculated for different kinds of systems, where the magnetic properties present a variation along the thickness in such a way that a magnetic texture is formed along the normal direction.

In the systematical study of ferromagnetic multilayers, the convergence of the system is firstly analyzed. Here, the idea is to explore the number of layers necessary to reach convergence and, thus, describe a continuously texturized magnetic film (where the magnetic texture is along the normal). Besides, different types of configurations were analyzed, namely: (i) set a weak exchange coupling in the middle of the layers, then (ii) study the case of a weak exchange coupling in the first two layers and strong anisotropy on the top layer, and finally, explore the case of (iv) thick ferromagnetic layers with an anisotropy profile along the thickness.

For the analysis, the reference material is permalloy. Hence, the magnetic parameters considered in the discussion are [13] $M_{\mathrm{s}} = 800$ kA/m for the saturation magnetization, and $A_{\mathrm{ex}} = 10$ pJ/m for the exchange constant. The exchange parameter $J$, associated with the interlayer exchange coupling, is written in terms of the constant $A_{\mathrm{ex}}$. This relation can be obtained by analyzing the transition from the discrete to the continuous case since if the number of sublayers increases, the dynamic properties of the continuous case are reached. Thus, if the number of layers is considerable, it can be demonstrated that $J = 2A_{\mathrm{ex}}/b$ [14]. Besides, in all cases it will assumed that the external field is applied along the $x$-axis ($\psi_H = 0$), while $y$ is an easy axis. Thus, the modulation of the magnetization between $\psi = 90°$ (easy direction) and $\psi = 0°$ (direction of the external field) will be systematically studied.

### 4.0.1 Convergence

To analyze the dynamic properties of the system, the convergence associated with the divisions is firstly studied. Hence, the behavior of the equilibrium angle $\psi$ for a sample of a total thickness $d_T = 50$ nm and $\mu_0 H_u = 500$ G are considered. In figure 4.1, the equilibrium magnetization and frequency as a function of field are illustrated. Here, it is observed that the systems present the same behavior if the number of divisions is $N = 20$ and 30. In the case of the frequency modes, the first two low-frequency modes has the same behavior. Therefore, one can conclude that the convergence is reached for $N = 20$.

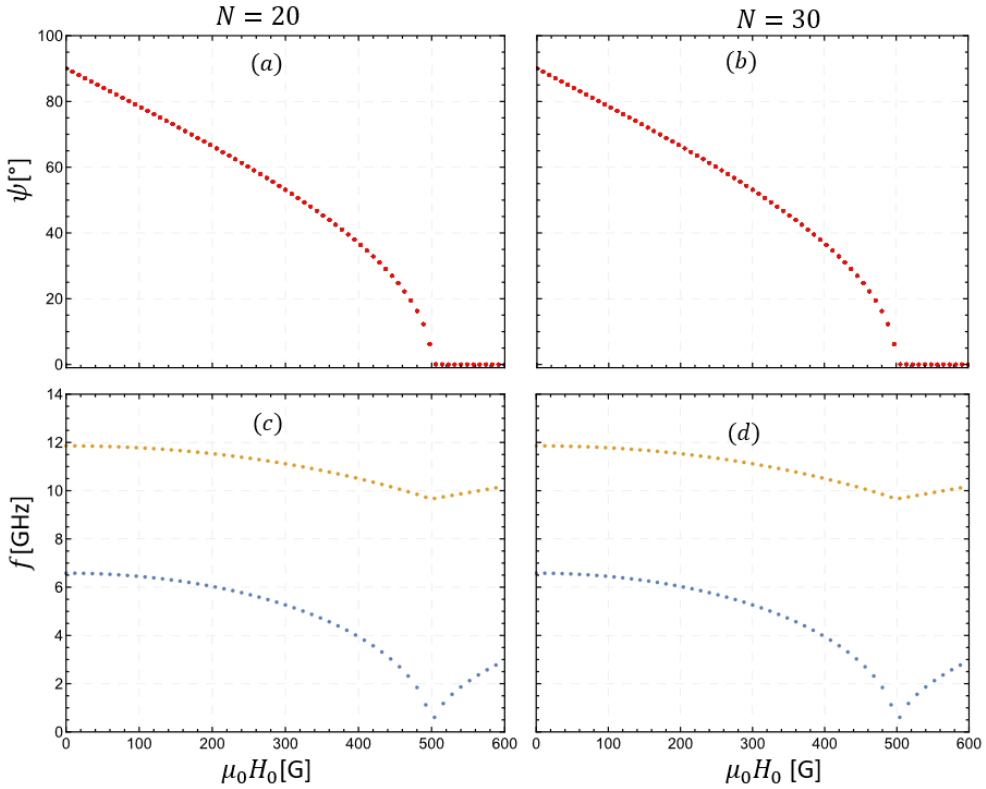


Figure 4.1: (a)–(b) Equilibrium angles for samples with different quantity of divisions, (a) $N = 20$ sublayers and (b) $N = 30$ sublayers. (c)–(d) Frequency as a function of field $H_0$.

If the high-frequency modes are considered, it is expected that they are sensitive to the number of the divisions, due to the number of nodes that they have along the thickness. Therefore, it is interesting to analyze the convergence of the these modes as a function of $N$. In figure 4.2 the cases $N = 20$, 30 and 40 are shown. Interestingly, one can observe that the convergence is rapidly reached for the low-frequency modes (up to the first eight low-frequency modes for $N = 20$). Nevertheless, for the high-frequency modes there is a discrepancy between the cases $N = 20$ and 30, for instance. In the same sense, the discrepancy also appear in the cases $N = 30$ and 40. Therefore, the divisions required to reproduce the continuous case are connected with the nature of the modes that one wants to analyze. For example, if the first three low-frequency modes are studied, then a division of $N = 20$ is enough to describe the dynamics of the system. Fortunately, in the most of the real cases, the low-frequency modes are of interest and hence the idea of calculating the static and dynamic properties with a small value of $N$ (number of divisions) works.

A similar analysis was realized for a sample of $d_T = 150$ nm of thickness. Figure 4.3 shows the convergence for such a case (150 nm). Here, one can observe a similar behavior than the thinner sample (50 nm). In fact, the convergence of the first eight modes is reached for the case $N = 20$. Note that the frequency range of the modes is lower than the previous case, because for a thicker ferromagnetic film the out-of-phase modes will have lower exchange energy. This means that the frequency of the modes is reduced.

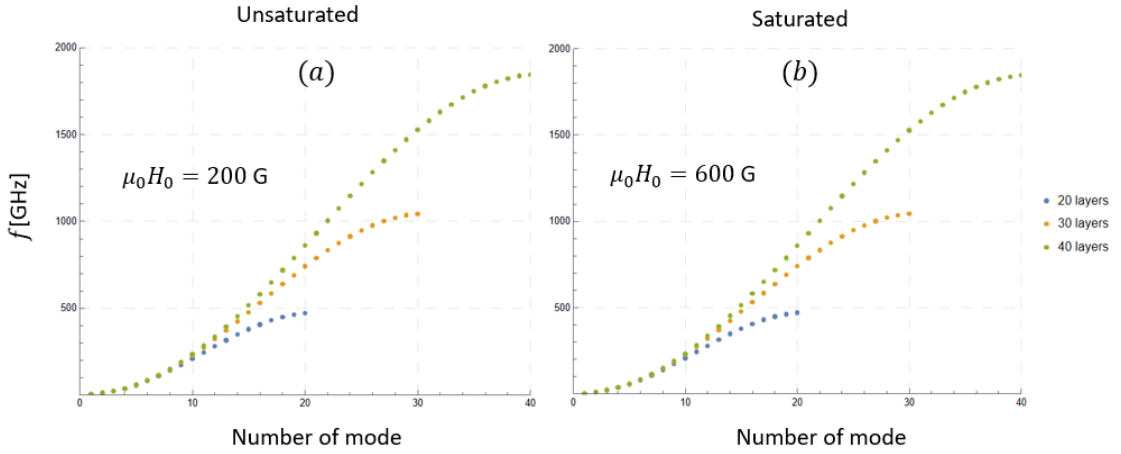


Figure 4.2: Frequency modes of sample $d_T = 50$ nm evaluated at (a) $\mu_0 H_0 = 200$ G and, (b) $\mu_0 H_0 = 600$ G. For these fields, the equilibrium states are evaluated before and after the saturation, respectively. Three divisions are considered in the calculations, namely $N = 20$, 30 and 40.

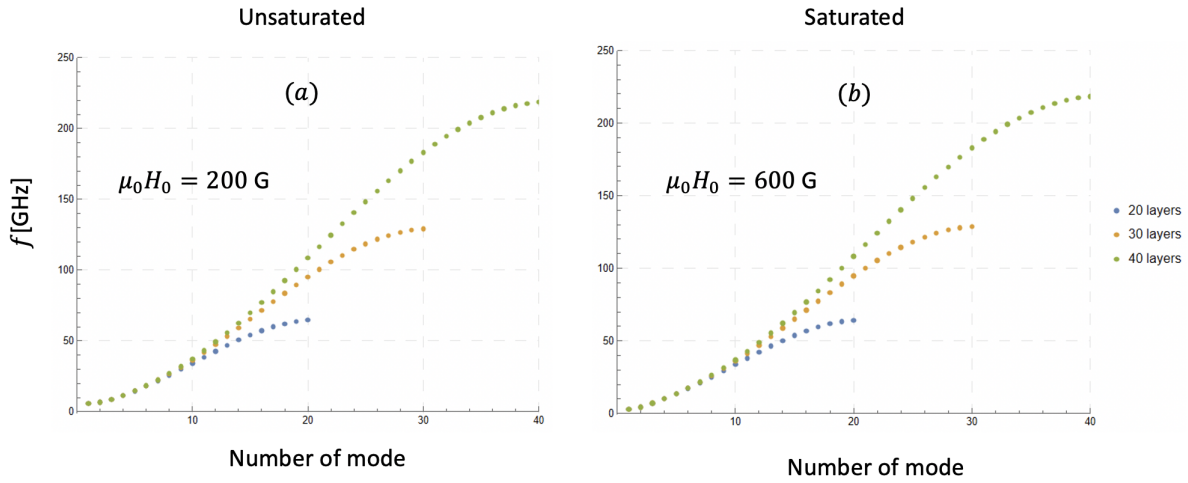


Figure 4.3: Frequency modes of case $d_T = 150$ nm. The fields are considered before and after the saturation, namely (a) $\mu_0 H_0 = 200$ G and, (b) $\mu_0 H_0 = 600$ G, respectively.

### 4.0.2 Weak exchange coupling in the middle of the layers

Now, the idea is to study unconventional cases. As the first example, weak coupling is set at the middle of the sample (at the middle of the thickness). For this purpose, it has been included a weak exchange interaction Jw = 0.005J at the thickness center, where J corresponds to the interaction of the rest of the layers ($J = 2A_{\text{ex}}/b$). Figure 4.4 shows the behavior of the frequency modes as a function of the external field. It is observed that the zero-order mode (low-frequency one) does not change significantly (see figures 4.4(a) and (c)). Nevertheless, the second normal mode reduces its dynamic energy or frequency remarkably. The explanation is related to the fact that the location where the weak exchange coupling is included matches with the node of the magnetization oscillation (see insets in figures 4.4(a) and (c)). Thus, consequently, it means that the out-of-phase oscillation will have low energy because the antiparallel dynamic magnetizations (around the node) present a considerably low exchange interaction. On the other side, if the total thickness increases (see figures 4.4(b) and (d)), it is observed that the second mode (the one that has a node at the center) reaches almost hybridizes with the fundamental one. This is expected because for thicker films, the out-of-phase modes decrease their frequency.

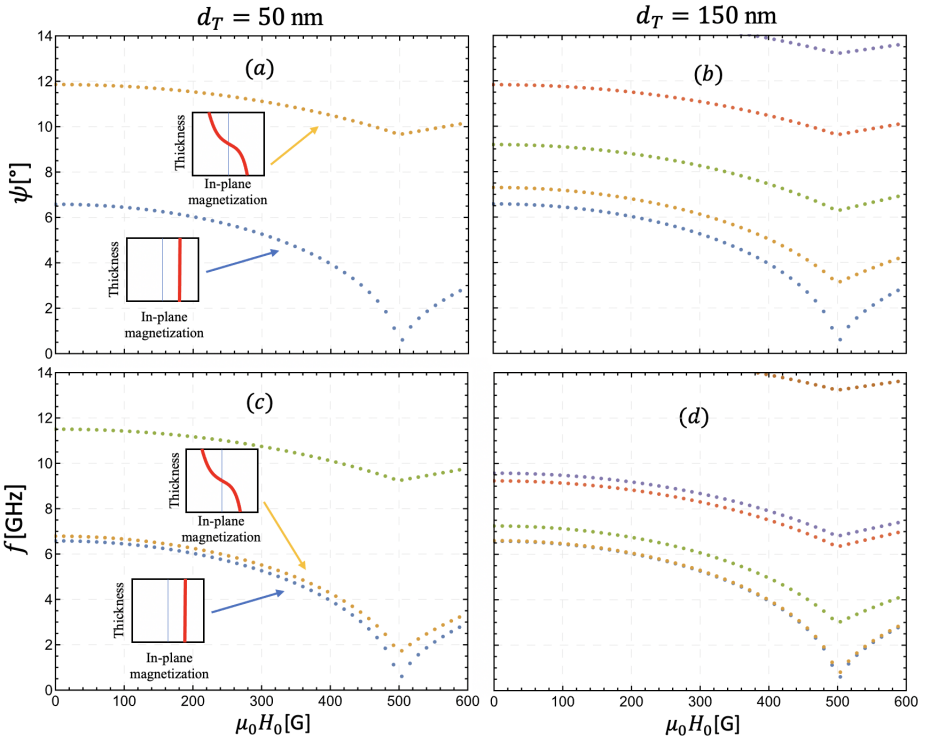


Figure 4.4: (a)–(b) Equilibrium angles for samples with different thickness, (a) 50 nm and (b) 150 nm. (c)–(d) Frequency as a function of field $H_0$.

### 4.0.3 Weak exchange coupling in the first two layers and strong anisotropy on the top layer

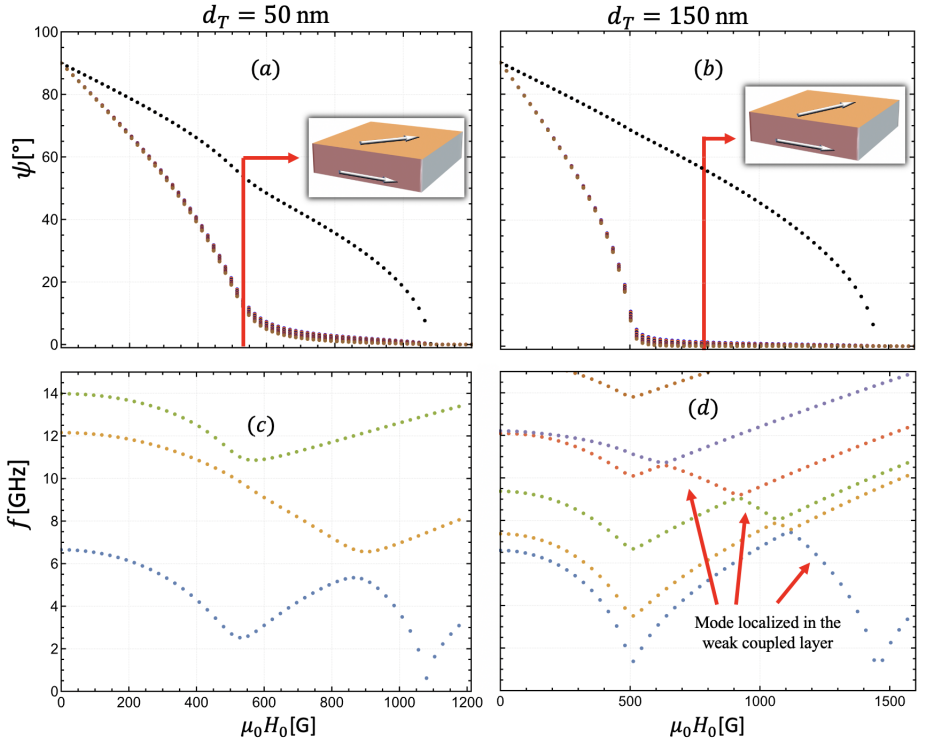


Figure 4.5: (a)–(b) Equilibrium angles for samples with different thickness, (a) 50 nm and (b) 150 nm. (c)–(d) Frequency as a function of field $H_0$.

The following case is similar to the previous one, but the weak coupling is given between the first two layers (1 and 2), while the first layer (or top layer) has a three times stronger anisotropy in comparison to the rest of the sample ($\mu_0 H_u = 1500$ G). From figure 4.5, it is possible to see two main falls of the angles, the first one is around $\mu_0 H_0 \approx 580$ G, which corresponds to the magnetic moments without the strong anisotropy. The other one fall around $\mu_0 H_0 \approx 1500$ G, where the entire sample reaches the saturation. This last behavior is associated with the layer that has strong anisotropy. On the other side, the dynamic behavior is also affected by the weak coupled layer. In figures 4.5(c) and (d), it is possible to observe that the mode located at the top layer (where the anisotropy is higher) crosses the rest of the bulk modes (modes excited in the bulk of the sample). Interestingly, for the thinner case (figure 4.5(c)), there is a coupling between the edge mode (mode located at the top layer) and the rest of the modes. This is attributed to the repulsion between modes. Nevertheless, for the thicker case ($d_T = 150$ nm), the modes are more uncoupled since they cross without repulsion. This is clearly observed in figure 4.5(d).

### 4.0.4 Thick layer with an anisotropy profile along the thickness

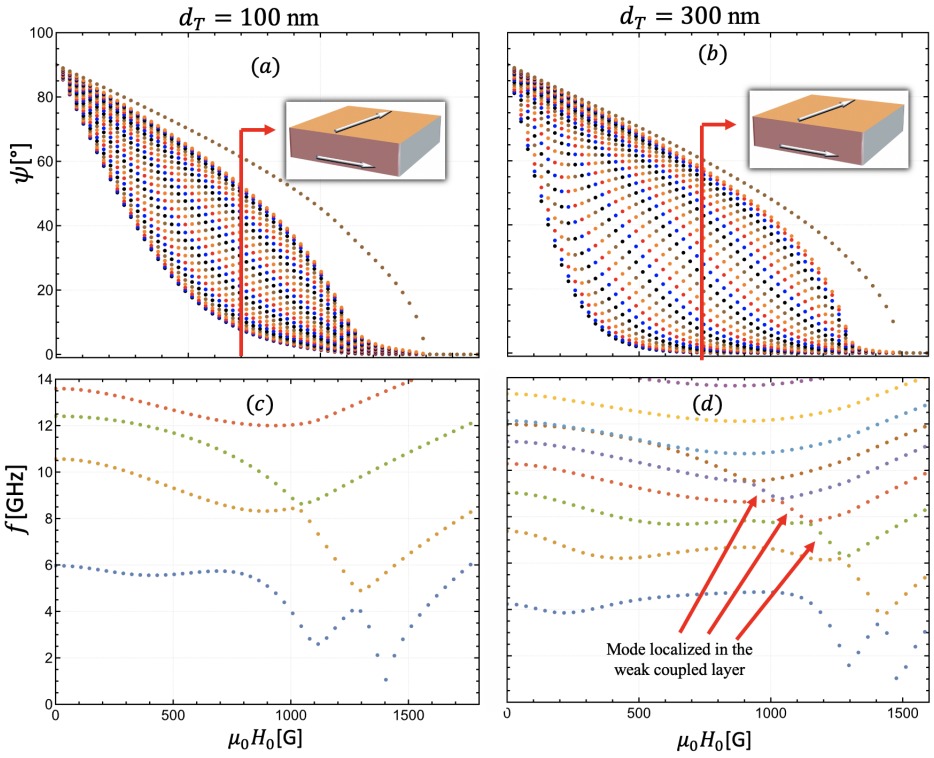


Figure 4.6: Equilibrium angles for samples with different thickness (a) 50 nm and (b) 150 nm

In this last case, an anisotropy profile along the thickness is considered where the anisotropy varies linearly from $\mu_0 H_u = 50$ G (top layer) to $\mu_0 H_u = 1500$ G (bottom layer). Besides, the bottom layer is weakly coupled with the rest of the layers ($J_w = 0.005J$). The static and dynamic behavior is depicted in the figure 4.6. From the equilibrium angles, it can be observed that the magnetization has a twisted or texturized state along the thickness. For instance, around $\mu_0 H_0 = 700$ G, the top magnetization makes an angle of 10 °, while for the bottom layer (the one with strong anisotropy) is around $\psi = 60$ °. The magnetization of the other layers rotates gradually between these two angles. So, this configuration represents a texturized ground state. It is basically reached due to the gradual modulation of the anisotropy along the thickness. Note that the thicknesses used in the calculations are several times the exchange length of the permalloy (around 5 nm), which is necessary to induce the texturized equilibrium state. For thin films, the exchange dominates, and even with an anisotropy variation, the magnetization will be homogeneous along the thickness. On the other side, the dynamics are notoriously influenced by the profile of the anisotropy. In figures 4.6(c) and (d), the behavior of these modes at low fields (before the saturation) evidences exotic variations that evidently are associated with the particular texturized ground state. It is important

to note that the coupling between the defect and the bulk modes decreases as the thickness of the sample increases (as in the previous case shown in 4.5) because such a defect layer (with weak coupling and strong anisotropy) becomes more insignificant for thicker films. Hence, one can conclude that the influence of the defects on the SW dynamics depends on the ratio between the thickness where the defect is located and the total thickness of the sample.

# Chapter 5

# Conclusions and future work

The present work has described a systematic study of ferromagnetic resonance for multilayers. The proposal is based on the advantages of magnonics in technology applications and explores the dynamical matrix method, which uses the geometry of the sample to simplify the calculations.

The method used consists of an eigenvalue problem to determine the system's frequency under the assumptions of the linear regime response and the small deviations of the magnetization.

As a result of this, the principal conclusions and observations of the developed work are the following:

1. The convergence of the system is independent of the quantity of the sublayers in the sample, it means it does not matter if the sample has twenty of thirty sublayers, the frequency for the first modes are equivalent.

2. A sample with a weak exchange coupling in the middle of the sample provokes a magnetic separation in the system because the location of the weakness matches with the node of the first oscillation mode. Indeed, the nature of this phenomenon is purely geometric, and it would work for other normal modes.

3. The case with weak exchange coupling and strong anisotropy in the first layers is interesting to analyze because it is an excellent approach to studying the defect mode, which is common in experimental results and gives a possible explanation of the phenomena.

Finally, in the light of the results and the developed ideas, future research will consider:

1. Introduce spin waves to the system, in that way, new energetic components are introduced, and interactions among sublayers change like dipolar energy.

2. Study the defect mode for the case out-of-plane within an isotropic plane.

3. Research about how the defect mode affects the line width due to the intersections between the defect and modes showed it could increase the width of the sample.

# Bibliography


[1] G.A. Melkov A.G. Gurevich. *Magnetization Oscillations and Waves.* CRC Press, London, 1996.

[2] Anjan Barman, Gianluca Gubbiotti, S Ladak, A O Adeyeye, M Krawczyk, J Gräfe, C Adelmann, S Cotofana, A Naeemi, V I Vasyuchka, B Hillebrands, S A Nikitov, H Yu, D Grundler, A V Sadovnikov, A A Grachev, S E Sheshukova, J-Y Duquesne, M Marangolo, G Csaba, W Porod, V E Demidov, S Urazhdin, S O Demokritov, E Albisetti, D Petti, R Bertacco, H Schultheiss, V V Kruglyak, V D Poimanov, S Sahoo, J Sinha, H Yang, M Münzenberg, T Moriyama, S Mizukami, P Landeros, R A Gallardo, G Carlotti, J-V Kim, R L Stamps, R E Camley, B Rana, Y Otani, W Yu, T Yu, G E W Bauer, C Back, G S Uhrig, O V Dobrovolskiy, B Budinska, H Qin, S van Dijken, A V Chumak, A Khitun, D E Nikonov, I A Young, B W Zingsem, and M Winklhofer. The 2021 magnonics roadmap. *Journal of Physics: Condensed Matter*, 33(41):413001, aug 2021.

[3] A. N. Bogdanov and U. K. Rößler. Chiral symmetry breaking in magnetic thin films and multilayers. *Phys. Rev. Lett.*, 87:037203, Jun 2001.

[4] A. Bogdanov and A. Hubert. Thermodynamically stable magnetic vortex states in magnetic crystals. *Journal of Magnetism and Magnetic Materials*, 138(3):255–269, 1994.

[5] Markus Garst, Johannes Waizner, and Dirk Grundler. Collective spin excitations of helices and magnetic skyrmions: review and perspectives of magnonics in non-centrosymmetric magnets. *Journal of Physics D: Applied Physics*, 50(29):293002, jun 2017.

[6] M. Labrune and L. Belliard. Stripe domains in multilayers: Micromagnetic simulations. *physica status solidi (a)*, 174(2):483–497, 1999.

[7] Carlos Javier Garcia Cervera. *Magnetic domains and magnetic domain walls.* New York University, 1999.

[8] Steven H. Simon. *The Oxford Solid State Basics / Steven H. Simon.* Oxford University Press, Oxford, first edition. edition, 2013.

[9] Daniel D. Stancil Anil Prabhakar. *Spin Waves - Theory and Applications.* Springer, New York, NY, 2009.

[10] J. M. D. Coey. *Magnetism and magnetic materials / J.M.D. Coey.* Cambridge University Press, Cambridge, 2010.

[11] David J Griffiths. *Introduction to electrodynamics; 4th ed.* Pearson, Boston, MA, 2013. Republished by Cambridge University Press in 2017.

[12] P. Alvarado-Seguel and R. A. Gallardo. Band structure of a one-dimensional bilayer magnonic crystal. *Phys. Rev. B*, 100:144415, Oct 2019.

[13] P. Malagò, L. Giovannini, R. Zivieri, P. Gruszecki, and M. Krawczyk. Spin-wave dynamics in permalloy/cobalt magnonic crystals in the presence of a nonmagnetic spacer. *Phys. Rev. B*, 92:064416, Aug 2015.

[14] R A Gallardo, P Alvarado-Seguel, T Schneider, C Gonzalez-Fuentes, A Roldán-Molina, K Lenz, J Lindner, and P Landeros. Spin-wave non-reciprocity in magnetization-graded ferromagnetic films. *New Journal of Physics*, 21(3):033026, mar 2019.